A Dual Polarized and High Gain X-/Ka Band Shared Aperture Antenna with High Aperture Reuse Efficiency

Mei, Peng; Zhang, Shuai; Pedersen, Gert Frølund

A Dual-Polarized and High-Gain *X*/*Ka*-Band Shared-Aperture Antenna with High Aperture Reuse Efficiency

Peng Mei, *Student Member, IEEE*, Shuai Zhang, *Senior Member, IEEE*, and Gert Frølund Pedersen, *Member, IEEE*

Abstract— **This paper describes a dual-polarized and high-gain shared-aperture antenna operating in *X* and *Ka*-band. The proposed shared-aperture antenna is implemented by combining a folded transmitarray (TA) antenna operating in *Ka*-band and a Fabry-Perot (FP) cavity antenna operating in *X*-band together. In this configuration, the shared aperture serves as a phase-shifting surface for the TA antenna, and as a partially reflective surface for the FP antenna simultaneously. Since both of the two antennas radiate into free space through the same physical aperture, the aperture reuse efficiency of the proposed antenna is 100%. A four-layered, metallic double-ring structure is selected as the unit cell (UC) to implement the shared aperture to fulfill the aforementioned requirements. It is found that the frequency responses of the UC in *X*- and *Ka*-band are highly independent, which can be controlled separately to facilitate the antenna design and optimization. Two dual-polarized patch antennas operating in *X* and *Ka*-bands are utilized to enable a dual-polarized manner of the proposed shared-aperture antenna. The simulated results reveal that the proposed antenna has the -10 dB bandwidth of 9.8-10.2 GHz and 26.5-29.0 GHz with the realized gain of 14.8 dBi (at 10 GHz) and 24.4 dBi (at 28 GHz) in two polarizations. All the simulations are experimentally verified.**

Index Terms— **Shared aperture, folded transmitarray antenna, Fabry-Perot antenna, perfect aperture reuse efficiency.**

I. INTRODUCTION

S HARED-APERTURE antennas are emerging antennas, attracting lots of attention and interests recently due to their unique advantages of dual-band/multi-band, compact size, low cost, low mass, high space utilization efficiency, etc [1]-[13], which can be potentially deployed and applied in synthetic aperture radar (SAR) [3], [7]-[9], satellite communications [11], and base station communications [12]. The shared-aperture antenna, by its name, is a kind of antenna that is usually composed of several antennas operating in different frequency bands together, where these antennas radiate into free space efficiently by sharing a partial or entire aperture. To this end, the keys to designing a shared-aperture antenna are to find out proper types of antennas and integrating them together in an efficient architecture, where the properties of these antennas usually determine the performance of the established shared-aperture antenna to some extent. There are some design considerations for a shared-aperture antenna: a). Polarization. Dual-polarization is preferred since it can provide polarization diversity and increase the traffic handling capacity of a system; b). Frequency ratio (FR), which is defined by the ratio of the highest and lowest frequency of a shared-aperture antenna. A large FR is reasonable, otherwise, a wideband antenna such as a wideband ridge horn antenna can replace a shared-aperture antenna in function; c). Aperture reuse efficiency, defined by the ratio of the actual radiation aperture areas of a shared-aperture antenna in different frequency bands. It should be emphasized here that when defining the aperture reuse efficiency, the shared aperture is essential for all sub antennas of a shared-aperture antenna.

A slot and slot arrays are one kind of the popular sub antennas to form a shared-aperture antenna [1]-[5]. In [1], the authors reported a shared-aperture antenna operating in *S/K*-band. In this design, the *S*-/*K*-band sub antennas were in the same layer, where the slot operating at *S*-band was embedded within the *K*-band slot arrays. A metasurface located above the sub antennas was served as the radiator of the *S*-band antenna but was transparent to the *K*-band antenna. A *L*-/*X*-band shared-aperture antenna was formed by etching crossed slots and the slot arrays on the surface of a metal cavity in an interleaved configuration [3], where the *L*-/*X*-band slot arrays radiate through different areas within the same aperture. The main drawbacks for such shared-aperture antennas based on slot and slot arrays (e.g., [1]-[5]) are single-polarization and a SIW-based feeding network is needed for high frequency to achieve high gain.

Patch antennas (or arrays) combining with feeding networks are another technique to design shared-aperture antenna with dual polarizations [6]-[10]. A triple-band shared-aperture antenna was reported in [9], where the authors employed patches with different sizes for *X*/*Ku*/*Ka*-band radiations. To excite the *X*/*Ku*/*Ka*-band patches in a dual-polarized manner, three complicated feeding networks are designed and configured in different layers, which would be lossy in the high

frequency. Such dual-polarized shared-aperture antennas (e.g., [6]-[10]) are achieved at the expense of lossy and complicated feeding networks.

Referring to the definition of aperture reuse efficiency, a shared-aperture antenna with an aperture reuse efficiency of 0.77 was reported in [5], where the authors served the radiating patch of a patch antenna operating at 3.5 GHz as the metal ground for the 60 GHz slot array antenna. A dual-band reflectarray in [11] achieved a perfect aperture reuse efficiency, where the unit cells are served as the phase-shifting elements in *X*- and *Ka*-band simultaneously. However, the dual-band reflectarray antenna suffers from the bulky volume (high profile) and high dependence of the two bands.

In this paper, a dual-polarized and high-gain *X/Ka*-band shared-aperture antenna is proposed with a high aperture reuse efficiency of 100%. The proposed shared-aperture antenna has a low profile and is formed by a folded transmitarray (TA) antenna in *Ka*-band and a Fabry-Perot (FP) antenna in *X*-band since both of the antennas have the similar geometries. To this end, it is required that the shared aperture should not only be served as phase-shifting surfaces for the TA antenna but also as a partial reflectance/transmission surface for the FP antenna. As a result, both of the antennas are radiating into free space through the physically same aperture, leading to a perfect aperture reuse efficiency. A four-layered, metallic double-ring structure is proposed as the unit cell (UC) to perform the shared aperture to fulfill the aforementioned requirements. The simulated results indicate the UC offers the phase-shifting abilities in *Ka*-band and partial reflectance/transmission in *X*-band simultaneously. Moreover, the frequency responses of the UC in *X*- and *Ka*-band can be controlled independently. Two dual-polarized patch antennas with very simple geometries, operating in *X*- and *Ka*-band, are designed to achieve the dual-polarization of the proposed shared-aperture antenna. The measured results reveal the -10 dB bandwidth of 26.7- 29.4 GHz and 9.75-10.2 GHz with the average isolation of around 15 dB and 30 dB between two polarizations, respectively. A realized gain of 13.8 dBi at 10 GHz and 23.6 dBi at 28 GHz of the proposed shared-aperture antenna are experimentally obtained as well. Besides, the performance of the shared-aperture design in two polarizations is highly consistent based on the measurements.

Compared with the existing work [1]-[11], it is obvious to conclude the contributions and advantages of the proposed shared-aperture antenna:

a). By fully taking advantage of working mechanisms and geometries of the folded TA antenna and FP antenna, both of the antennas radiate into free space through the same physical aperture, leading to a perfect aperture reuse efficiency of 100%;

b). Without any complicated feeding networks, it is very easy to achieve high gains and dual-polarization while keeping a relatively low profile;

The outlines of the paper are organized as follows: Section II explains the concept of the proposed shared-aperture antenna; the desired UC is analyzed and its frequency responses are fully elaborated in section III; the implementations of the proposed shared-aperture antenna operating in *X* and *Ka*-band are presented in Section IV; the proposed shared- aperture antenna is fabricated and measured, which is also compared with the simulated results in Section V. Some remarkable conclusions are drawn in Section VI.
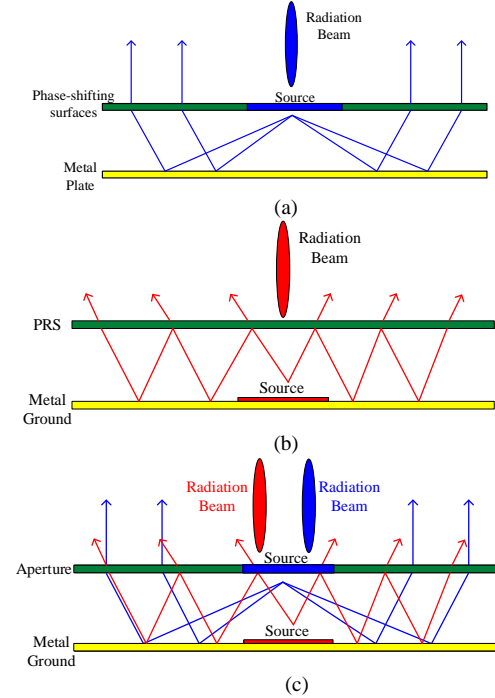

Fig.1. Evolutions of the proposed shared-aperture antenna. The configurations of (a) a folded transmitarray antenna, (b) a Fabry-Perot antenna, and (c) the proposed shared-aperture antenna.

II. CONCEPT

An evolutional diagram is presented to explain the concept of the proposed shared-aperture antenna. Fig. 1 (a) is the configuration of a folded TA antenna. It consists of a metal plate, phase-shifting surfaces, and a feeding source, where the feeding source and the phase-shifting surfaces are located on the same plane. A focused beam at broadside would be achieved when the electromagnetic waves radiating from the feeding source propagate through the phase-shifting surfaces. In contrast, Fig. 1 (b) shows the corresponding configuration of a FP resonant antenna, where a partially reflective surface is placed above a feeding source with a certain separation. Electromagnetic waves radiating from the feeding source would experience multiple reflections between the PRS and metal ground, where the separation between them is decided to make the electric fields at the aperture of PRS in-phase so that a high gain can be achieved.

From Fig. 1(a) and (b), it is observed that the geometries and configurations of the folded TA antenna and the FP antenna are very similar to each other, which both of the two antennas include a feeding source, a metal ground and a superstrate located above a metal ground with a separation. To this end, it inspires one to combine the two antennas together to realize a

shared-aperture antenna as shown in Fig. 1 (c), where the folded TA antenna and FP antenna are responsible for radiating in the high- and low-frequency band, respectively. Since both of the folded TA and the FP antennas radiate into free space through the same physical aperture, a 100 % aperture reuse efficiency is obtained for the proposed shared-aperture antenna.

To achieve the proposed shared-aperture antenna, one of the challenges is to find out a proper UC to implement the shared aperture. Specifically speaking, the desired shared aperture is required to be served as a phase-shifting surface with a small attenuation in the high-frequency band for the folded TA antenna and show partially reflective/transmissive properties in the low-frequency band for the FP antenna simultaneously. Moreover, independent controls of the frequency responses of the shared aperture in the low- and high-frequency band are also preferred.
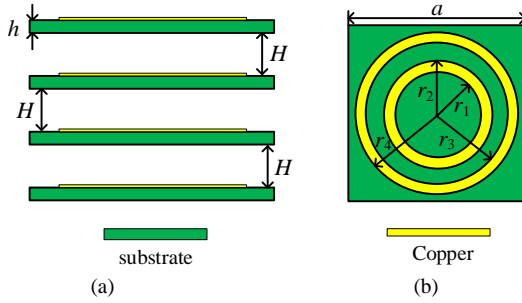

Fig. 2. The geometries of the UC. (a). Side view. (b). Front view. (h = 0.305 mm, H = 2.5 mm, r_4 = 2.25 mm, r_3 = 1.75 mm, r_2 - r_1 = 0.5 mm)
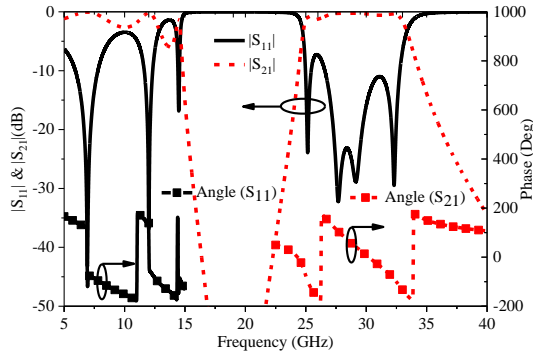

Fig. 3. The S-parameter of the UC. (r_4 = 2.25 mm, r_3 = 1.75 mm, r_2 = 1.15 mm, r_1 = 0.5 mm)

III. UNIT CELL DESIGN AND ANALYSIS

A. Configuration of the unit cell.

Fig.2 presents the geometries of the proposed UC. It consists of four identical layers, where the metallic double-ring patterns are printed on each supporting substrate. The supporting substrate is Rogers RO4003C with a thickness of 0.305 mm, a dielectric constant of 3.55, and a loss tangent of 0.0027. Considering that the UC will serve as a phase-shifting element at 28 GHz, the periodicity of the UC (a) and air separation (H) between each layer are 5 mm and 2.5 mm (corresponding to $\lambda/2$

and $\lambda/4$ at 28 GHz approximately), respectively. The dimensions of the metallic double-ring are initially given as follows: r_4 = 2.25 mm, r_3 = 1.75 mm, r_2 = 1.05 mm, and r_1 = 0.55 mm. The S-parameters of the UC are simulated and evaluated by using CST Microwave Studio software, where periodic boundary conditions (PBC) are imposed on the UC to emulate an infinite surface. Fig. 3 shows the S-parameters of the UC from 5 to 40 GHz with a normal incidence wave. It is found that the UC can be regarded as a phase-shifting element in the high-frequency band from 24 to 34 GHz, and as a partial reflectance/ transmission element in the low-frequency band from 8 to 12 GHz or 13 to 14 GHz, which is a candidate for the desired shared aperture implementation.

B. High-frequency analysis

It has been proved that a four-layered, metallic double-ring (square) UC is typically employed as a phase-shifting element for a TA antenna design since it can not only provide a full phase-cycle (2π) but also offer an acceptable attenuation (less than 1dB) [14]. To figure out the working mechanisms of the UC well, a single layer of the UC is investigated from its equivalent circuit and current distributions. Fig. 4 (a) gives the equivalent circuit of the single-layer double-ring structure, where two shunt LCs caused by the outer and inner metallic rings are in parallel. It is also known that a shunt LC shows a bandstop frequency response at a specific frequency that is usually calculated by $f = 1/(2\pi\sqrt{LC})$, resulting in a transmission zero in the frequency spectrum. Since the dimensions of the outer and inner metallic rings are different, the frequencies of the two transmission zeros are distinguished accordingly. Between the two transmission zeros, there exists a reflection pole [15], which has been verified by the simulated results. Therefore, it can be sufficiently predicted that the proposed UC can generate four reflection poles since it is formed by cascading four identical layers [15]. The theoretical analysis is highly consistent with the simulated results shown in Fig. 3, where four reflection poles are observed in the high-frequency band. The current distributions on the metallic double-ring at the reflection pole are presented in Fig. 4 (b), where it is observed that currents are mainly concentrated in the outer periphery of the inner ring and inner periphery of the outer ring. The current distributions on the metallic double-ring would be served as a guideline to manipulate the frequency responses of the UC in the low- and high-frequency band.

Based on the equivalent circuit and current distributions, there are two possible techniques to adjust the frequency responses of the UC in the high-frequency band: one is to tune the radius of the inner ring with other parameters fixed, and the other is to modify the radius of the outer ring with other parameters fixed. Here, we adopt the former one to manipulate the frequency responses of the UC in the high-frequency band since the outer ring has a relatively large physical dimension that is expected to be employed to control the frequency responses in the low-frequency band. Here, we vary the radius of the inner ring but keep its width. Fig. 5 presents the amplitude

of S_{11}, reflection phases, and transmission phases of the UC with different values of r_2. It is observed that the passband is shifting toward higher frequencies when the value of r_2 decreases, while the frequency responses in the low-frequency band (from 5 to 15 GHz) are almost the same.
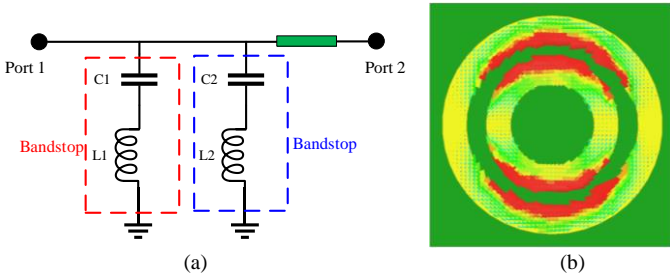

Fig. 4. The single layer of the proposed unit cell. (a). Equivalent circuit. (b). Current distributions on the double rings at the reflection pole.
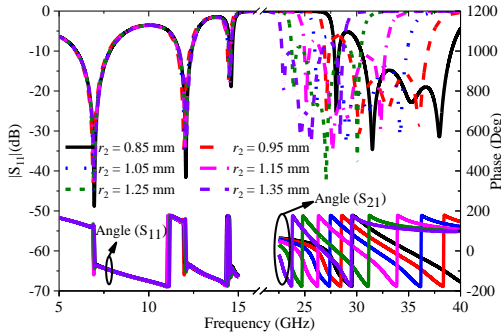

Fig. 5. The reflection coefficients of the proposed UC with different values of r_2. ($h = 0.305$ mm, $H = 2.5$ mm, $r_4 = 2.25$ mm, $r_3 = 1.75$ mm, $r_2 - r_1 = 0.5$ mm)
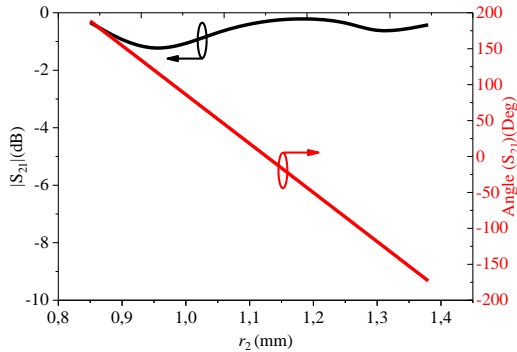

Fig. 6. The simulated transmission amplitude and phase of the UC with different values of r_2 at 28 GHz. ($h = 0.305$ mm, $H = 2.5$ mm, $r_4 = 2.25$ mm, $r_3 = 1.75$ mm, $r_2 - r_1 = 0.5$ mm)

It is also observed that the transmission phases of the UC vary regularly with a different value of r_2 as shown in Fig. 5, which can offer a full phase-cycle (2π) transmission phase coverage. The transmission amplitude and phase of the UC at 28 GHz with different values of r_2 extracted from Fig. 5 are plotted to further check its abilities to be served as a phase-shifting element. From Fig. 6, it is observed that a full phase-cycle is achieved with an average transmission attenuation of less than 1.0 dB when the value of r_2 varies from 0.85 to 1.40 mm.

C. Low-frequency analysis

As we know, FP antennas are a kind of resonant antennas, composed of a superstrate generally named PRS and a feeding source. The PRS is typically formed by lots of UCs periodically distributed or pure dielectric substrates [16]-[18]. The main consideration for a PRS is that the transmission/reflection phase and the reflective/transmissive amplitude on any position of it should be the same even if the PRS is not implemented by periodically distributed identical UCs. Then, by calculating the separation between the PRS and the feeding source, it is expecting to make the electric fields on the PRS aperture in-phase to achieve high gain at a certain frequency. In our design, the UCs to construct the PRS are not physically identical since the value of r_2 is required to be varied to fulfill the desired phase compensations for the folded TA antenna in the high-frequency band. However, such non-identical UCs can still work for a PRS implementation since both of the reflective/ transmissive amplitudes and transmission/reflection phases remain the same, which will be further explained in the following.

In Fig.5, it is observed that the reflection amplitudes and phases of the UC in the low-frequency band (from 5 to 15 GHz) are extremely stable when the value of r_2 varies from 0.85 to 1.40 mm. It should further check the transmission phases of the UC in the low-frequency band with different values of r_2. To this end, the reflection amplitude, reflection phase, and transmission phase of the UC at 10 GHz are plotted with different values of r_2. As seen in Fig. 7, the reflection amplitude, reflection phase, and transmission phase of the UC is around -3.5 dB, -151.0 deg, and 130 deg when the value of r_2 varies from 0.75 to 1.45 mm, respectively. The variations of reflection amplitude, reflection phase, and transmission phase are 0.08 dB, 1.6 deg, and 1.0 deg, respectively. The simulated results in Fig. 5 and Fig. 7 indicate the high feasibility of implementing to a PRS with the designed UCs for a FP antenna even though they are not physically identical.

The approaches to control the UC's frequency responses in the low-frequency band will be discussed in the following to provide detailed instructions and guidelines for the FP antenna design. Since the dimension of the inner ring has been used to obtain a full phase-cycle in the high-frequency band, we focus on tuning the dimension of the outer ring to adjust the UC low-frequency responses. As seen in Fig. 4(b), the currents are mainly concentrated on the inner periphery of the outer ring. We can expect the UC high-frequency responses should be maintained when the values of r_3, r_1, and r_2 are fixed, while the values of r_4 can potentially adjust the UC low-frequency responses. Here, we introduce and validate the following two approaches:

a). Varying the values of r_4 of every layer of the UC simultaneously while keeping the other parameters fixed. As seen in Fig. 8, the operating band shifts toward lower frequencies with the increment of r_4 while the high-frequency responses keep almost identical;

b). Only varying the values of r_4 of the second and third layers

while keeping the values of r_4 of the first and fourth layers of the UCs and the other parameters fixed. As observed in Fig. 9, the operating bandwidth of the UCs in the low-frequency band is broadened with r_4 decreasing, and the frequency responses in the high-frequency band are still nearly the same.

From Fig. 5, Fig. 8 and Fig. 9, it can be concluded that the frequency responses of the UCs in X- and Ka-band are highly independent with each other, and can be controlled separately by adjusting the specific parameters. This is a very important feature to ease the shared-aperture antenna design.
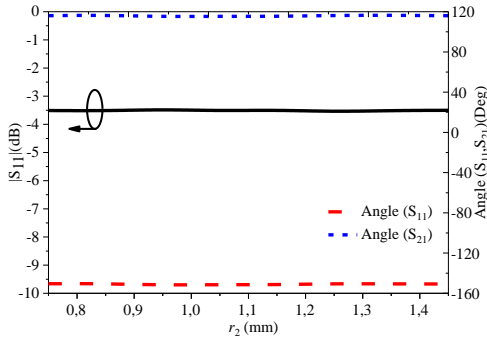

Fig. 7. The reflection amplitude, reflection phase and transmission phase of the UC at 10 GHz when the value of r_2 varies from 0.75 to 1.45 mm
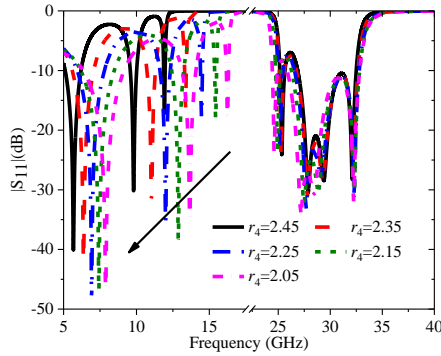

Fig. 8. The reflection coefficients of the UC when the value of r_4 varies from 2.05 to 2.45 mm with the other parameters fixed. (h = 0.305 mm, H = 2.5 mm, r_3 = 1.75 mm, r_2 = 1.05 mm, r_1 = 0.55 mm)
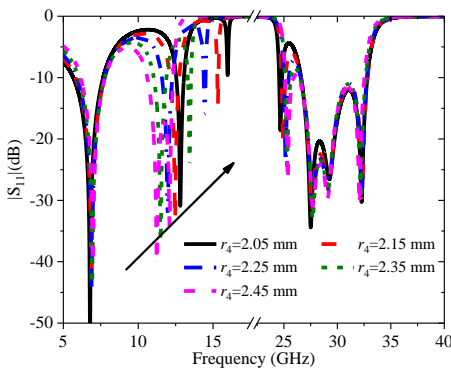

Fig. 9. The reflection coefficients of the UC when the value of r_4 varies from 2.05 to 2.45 mm with the other parameters fixed.

IV. SHARED-APERTURE ANTENNA IMPLEMENTATION

Since the UCs to construct the shared aperture are axially symmetrical, the shared aperture is feasible for dual- and circularly-polarized applications when the feeding sources of the shared-aperture antenna is dual- or circularly-polarized. In this section, a dual-polarized shared-aperture antenna is mainly investigated and presented. Two dual-polarized feeding sources are utilized for the proposed shared-aperture antenna to realize dual-polarization. According to the configurations shown in Fig. 1, the feeding source operating at 28 GHz would be integrated with the shared aperture. Since the shared aperture is a four-layered structure, there are three possible solutions to deploy the feeding source operating at 28 GHz as shown in Fig. 10. The feeding source can be located at either the first or the fourth layer of the shared aperture. It should be noted that the air separation between the first layer and the metal ground is determined by the FP antenna operating in the low-frequency band, which is chosen to make the electric fields on the shared aperture in-phase to realize high gain. If the distance is small, it would affect the reflection coefficient of the proposed shared-aperture in the high-frequency band. On the other hand, the feeding source operating at 28 GHz is fed with our available MMPX connectors [as shown in Fig. 11(c)] that have large footprints, resulting in the difficult assembling with the shared aperture if the feeding source is mounted on the first layer.

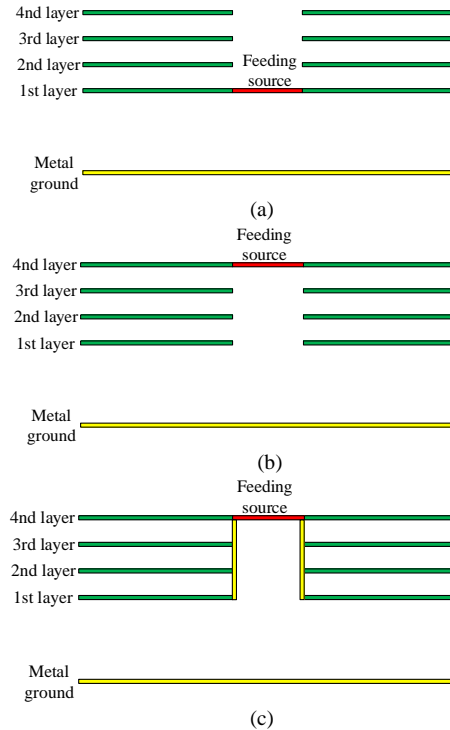Fig. 10. Three solutions to place the feeding sources in the shared aperture. The feeding source is located at: (a) the first layer, (b) the fourth layer without a metal cavity, and (c) the fourth layer with a metal cavity.

Alternatively, the feeding source can be located at the fourth layer as shown in Fig. 10 (b). In this configuration, there is much space for MMPX connectors assembling. However, it suffers

from a disadvantage that the remaining three layers (1st, 2nd, 3rd layer) would affect the radiation patterns of the feeding source and the perturbations are difficult to predict and evaluate, leading to some effects on the final radiation performance of the shared-aperture antenna in the high-frequency band. To solve this problem, a metal cavity is mounted to shield the feeding source from electromagnetic interferences with the remaining three layers as shown in Fig. 10 (c). Furthermore, the metal cavity can constrain the electromagnetic fields and make the radiation patterns of the feeding source more symmetrical.
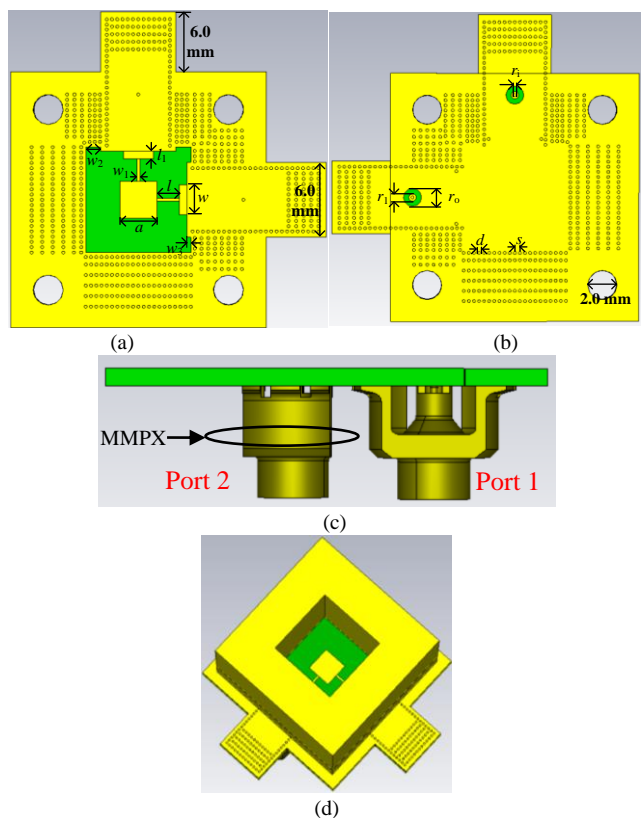

(a)
(b)
(c)
(d)

Fig. 11. The geometries of the dual-polarized SIW-based antenna. (a). Front view. (b). Back view. (c). Side view. (d). Perspective view with a metal cavity.

A. Dual-polarized SIW-based patch antenna at 28 GHz

The geometries of the dual-polarized SIW-based patch antenna are shown in Fig. 11. The substrate used here is also Rogers RO4003C with a dielectric constant of 3.55, and a loss tangent of 0.0027. To obtain a wider bandwidth, a thickness of 0.813 mm is adopted. The shape of the radiating patch is selected as a square to make the resonant frequencies the same in two polarizations. In order to excite the square patch antenna efficiently, a SIW to microstrip line transition and a quarter-wavelength impedance transformer are introduced. A coaxial to SIW transition is also adopted to feed the SIW cavity. The dimensions of the square patch are modified to make it resonant at 28 GHz. The height of the metal cavity exactly fits the total thickness of the shared aperture as shown in Fig. 11 (d). Fig. 12 (a) shows the S-parameters of the dual-polarized SIW-based patch antenna, where the -10 dB bandwidth is from 26.9 to 29.4 GHz with an absolute bandwidth of 2.5 GHz. The isolation

between the two ports is better than 15 dB at 28 GHz.

The radiation patterns of the dual-polarized SIW-based patch antenna are simulated at 28 GHz. As seen in Fig. 12 (b), the -10 dB gain edge tapers in E- and H-plane are very close, leading to a beamwidth of 150 and 137 degrees, respectively. Even though the 10 dB beamwidths in E- and H-plane are not exactly identical, they are feasible as a feeding source for a folded transmitarray antenna. The simulated peak realized gain is 7.74 dBi at 28 GHz. Besides, the 10 dB beamwidths of the dual-polarized SIW-based patch antenna are also checked from 26.5 to 29.5 GHz, which are 143-153 degrees and 136-140 degrees in E- and H-plane, respectively.
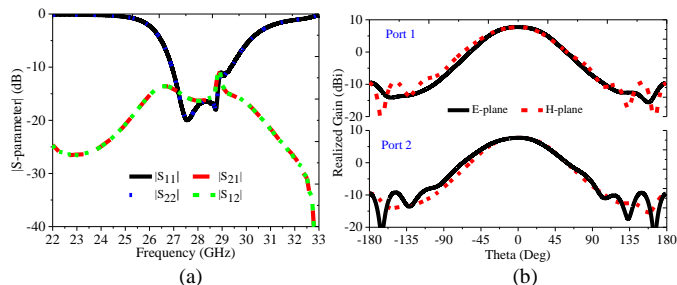

(a)
(b)

Fig. 12. (a). S-parameter of the dual-polarized SIW-based patch antenna. (b). The simulated co-polarizations of the dual-polarized SIW-based patch antenna at 28 GHz with port 1 and 2 excited, respectively.
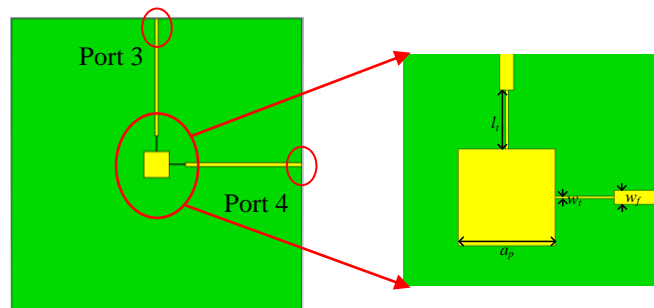

Fig. 13. Geometries of the dual-polarized patch antenna at 10 GHz.
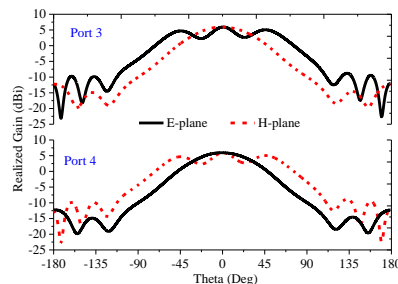
Fig. 14. The simulated co-polarizations of the dual-polarized patch antenna at 10 GHz with port 3 and 4 excited, respectively.

B. Dual-polarized patch antenna at 10 GHz

The geometries of the dual-polarized patch antenna at 10 GHz are shown in Fig. 13. The side feeding technique is adopted to feed the square patch for convenient measurements. Likewise, a quarter-wavelength impedance transformer is also used to achieve a good impedance match. The dimensions of the square

patch are roughly determined to make it resonant around 10 GHz since the final reflection coefficient would be slightly different with the counterpart of a single dual-polarized patch antenna when it is served as a feeding source for the proposed shared-aperture antenna in the low-frequency band because a superstrate (the shared aperture) is located above the patch antenna with a certain separation.

The simulated radiation patterns of the dual-polarized patch antennas are also presented at 10 GHz. Here, we choose the dimension of the metal ground consistent with the size of the shared aperture. It is observed in Fig. 14 that the radiation pattern in E-plane is not as good as the counterpart in H-plane at 10 GHz since the relatively large size of a metal gound usually affects the radiation patterns of a patch antenna as thoroughly investigated in [19], [20]. The simulated peak realized gain of the dual-polarized patch antenna is 5.9 dBi at 10 GHz. The radiation patterns are also checked at frequencies of 9. 75 and 10.25 GHz. The simulated results indicate radiation patterns of the dual-polarized antenna at frequencies of 9.75 and 10.25 GHz highly consitent with that at 10 GHz. Since the dual-polarized patch antenna is served as a feeding source for the proposed shared-aperture antenna in the low-frequency band. Even though the radiation patterns in E-plane are not ideal, the final radiation patterns of the proposed shared-aperture antenna are improved significantly at 10 GHz, which will be presented in the next subsection.

C. Implementation of the proposed shared-aperture antenna.

A shared-aperture antenna is constructed with the proposed UCs and two dual-polarized feeding sources. The size of the shared aperture is 85 mm × 85 mm, corresponding to 17 × 17 UCs in *x*- and *y*-directions. Firstly, the air separation between the metal ground and first layer of the shared aperture is determined by the following equation [21]:

$$-2\frac{2\pi}{\lambda}h - \varphi_{PRS} - \varphi_{Ground} = 2n\pi, n = 0, \pm 1, \pm 2, \pm 3, ... \quad (1)$$

where φ_{PRS} and φ_{Ground} are the reflection phases of the shared aperture and the metal ground at 10 GHz, respectively. Based on the reflection phase of the UC at 10 GHz, it is calculated that the air separation *h* equals 17.0 mm.

Once the air separation is determined, the phase compensation plane for the folded TA antenna is also decided accordingly. It should be mentioned here that the far-field zones of the two feeding sources) at 10 and 28 GHz are calculated according to the equation of d = 2D^2/λ, where D is the length or diameter of an antenna, λ is the wavelength. It is found that the far-field distances of the two feeding sources at 10 and 28 GHz are 7.6 and 2.24 mm, respectively. According to the calculated air separation of 17.0 mm, the shared aperture is located at the far-field zone of both the two feeding sources. Therefore, it is reasonable to only consider the radiation patterns (far-field) of the two feeding sources shown in Figs. 12 and 14.

Due to the slightly structural asymmetry of the dual-polarized feeding source at 28 GHz shown in Fig. 11 (radiation patterns in

E- and H-plane are not exactly identical), it can be reasonably predicted that the phase distributions on the phase compensation plane should be slightly different when port 1 or port 2 is excited, respectively. On the other hand, it should be noted that each single UC cannot provide two different transmission phases simultaneously. To this end, the average value of the final transmission phase is calculated as:

$$\varphi_{Final} = \frac{\varphi_1(i,j) + \varphi_2(i,j)}{2} \quad (2)$$

where $\varphi_1(i,j)$ and $\varphi_2(i,j)$ are desired transmission phases at the same UC with a position of (i, j) when port 1 and port 2 are excited, respectively. The adoption of the average value of the two transmission phases can minimize the difference of realized gain of the shared-aperture antenna in two polarizations. Fig. 15 plots the final phase distributions on the phase compensation plane. Based on the phase distributions, the final shared aperture is established with the proposed UCs according to the relation shown in Fig. 6.

The radiation patterns of the proposed shared-aperture antenna are simulated and evaluated at 10 GHz and 28 GHz, respectively. When one port is excited, the remaining ports are all terminated with matching loads. As shown in Figs. 16, the realized gain is 14.8 dBi at broadside when port 3 or 4 is excited at 10 GHz. At 28 GHz, the boresight realized gains are 24.4 dBi when port 1 or 2 is excited.
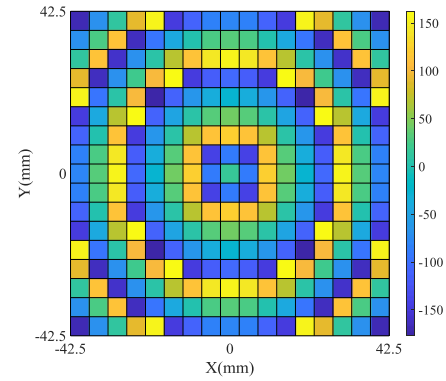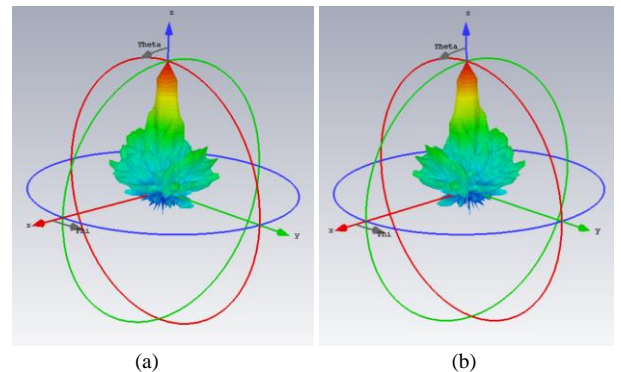

Fig. 15. The final phase distributions on the phase compensation plane at 28 GHz.

(a)   (b)
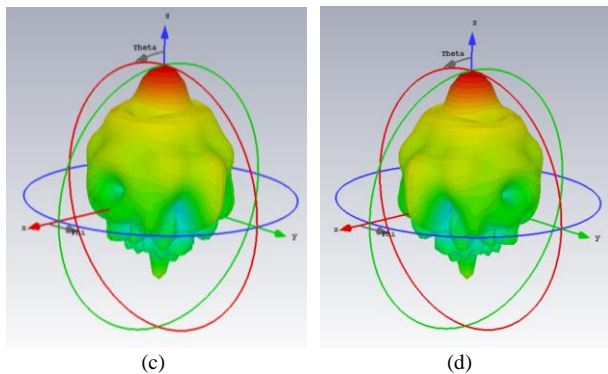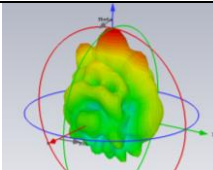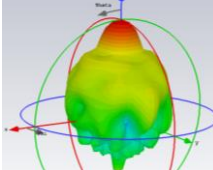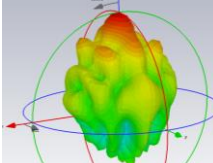
(c)   (d)

Fig. 16. The simulated 3D radiation patterns of the proposed shared-aperture antenna when different ports are excited at 10 GHz. (a). Port 1 is excited. (b). Port 2 is excited. (c). Port 3 is excited. (d). Port 4 is excited.

For a FP antenna, the gain is mainly associated with the reflective/transmissive amplitude and the aperture size of the PRS [21]. As stated in section III, the reflective/transmissive amplitude of the UC can be controlled independently in the low-frequency band. Here, the realized gains of the proposed shared-aperture antenna at 10 GHz are compared with three different reflective/transmissive amplitudes of the PRS as tabulated in Table I. It is observed that when the reflective amplitude is -3.50 dB, the proposed shared-aperture antenna has an optimal radiation pattern under a fixed shared aperture size (85 mm×85 mm), and also has the smallest air separation at 10 GHz.

Table I. Radiation performance comparisons of the proposed shared-aperture antenna with three different reflection/transmission amplitudes of the shared-aperture.

|	R-A (dB)	R-P (Deg)	A-S (mm)	R-G (dBi)	3D radiation pattern at 10 GHz
#1	-1.4	-103.4	17.0	14.9	
#2	-3.5	-150.9	16.2	14.8	
#3	-5.94	-94	18.6	13.7	

R-A: reflection amplitude; R-P: reflection phase; A-S: air separation; R-G: realized gain.

Table II. The dimension of the proposed shared-aperture antenna. (Unit: mm)

a	l	l_1	w	w_1	w_2	w_3	r_i
2.45	1.5	0.5	2.0	0.2	1.0	0.275	0.4
r_o	r_1	d	s	a_p	w_t	l_t	w_f
1.23	0.5	0.2	0.35	7.56	0.2	4.6	1.1

V. MEASUREMENT AND DISCUSSIONS

In this section, the proposed shared-aperture antenna is fabricated with the dimensions as listed in Table II and measured. Fig. 17 gives photographs of dual-polarized antennas, the proposed shared-aperture antenna and its different layers. All boards are produced by printed circuit board (PCB) technologies. There are 8 air holes with diameters of 3 mm uniformly distributed in the edges of every board for alignment. In order to support four-layered phase-shifting surfaces, some lightweight foams with relative permittivity of approximately 1.00 and required thicknesses are inserted between adjacent layers to make layers parallel with each other. It has been verified from the simulated results that the performance of the proposed shared-aperture antenna is still maintained when the relative permittivity of the foam is varied from 1.00 to 1.10 with an interval of 0.05 or the exact separation between layers is slightly bigger or smaller than the required one. The metal cavity is produced with CNC (computer numerical control) milling technologies [22]. Because the thickness of the substrate of the dual-polarized patch antenna at 10 GHz is only 0.508 mm, a metal plate with a thickness of 5 mm is also produced with mechanical milling technologies to be attached under the dual-polarized patch antenna at 10 GHz for supporting. The separation between the shared aperture and the dual-polarized patch antenna at 10 GHz is fixed with some metallic pillars with certain thicknesses.

(a)   (b)

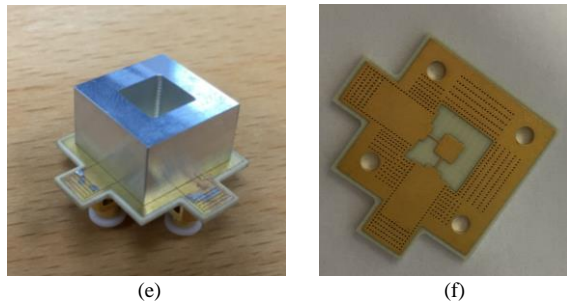(c)   (d)
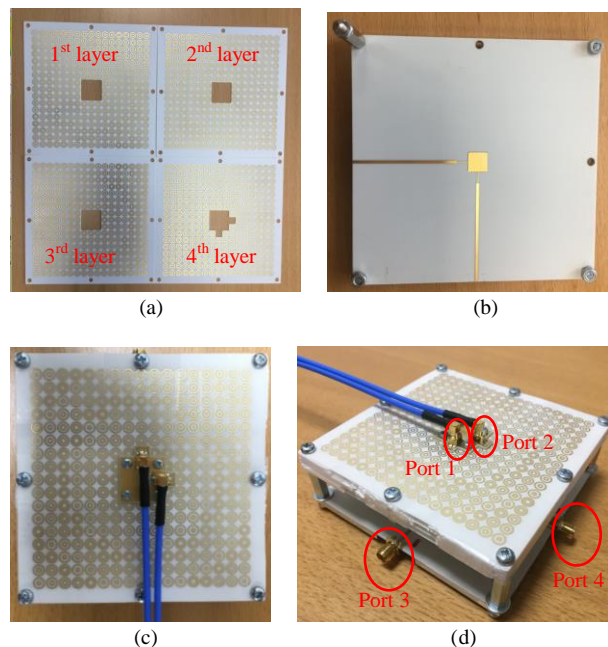
Fig. 17. Prototypes of the proposed shared-aperture antenna. (a). The front view of the four layers used to construct the shared aperture. (b). Front view of the dual-polarized patch antenna in the low-frequency band. (c). Front view of the proposed shared-aperture antenna. (d). Perspective view of the proposed shared-aperture antenna. (e). Perspective view of the dual-polarized SIW-based patch antenna in the high-frequency band. (f). Front view of the dual-polarized SIW-based patch antenna in the high-frequency (metal cavity is not shown here) (Notes: Port 1 and Port 3 have the same polarization, Port 2 and Port 4 have the same polarization.)
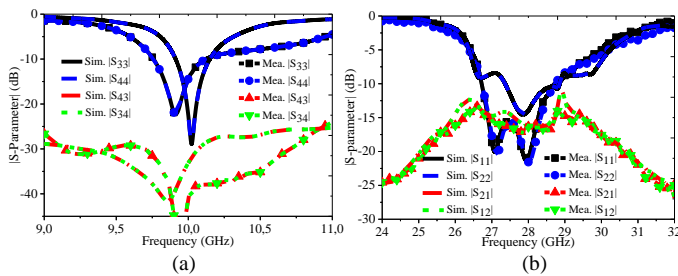

Fig. 18. The measured and simulated S-parameter of the proposed shared-aperture antenna. (a). In the low-frequency band. (b). In the high-frequency band.
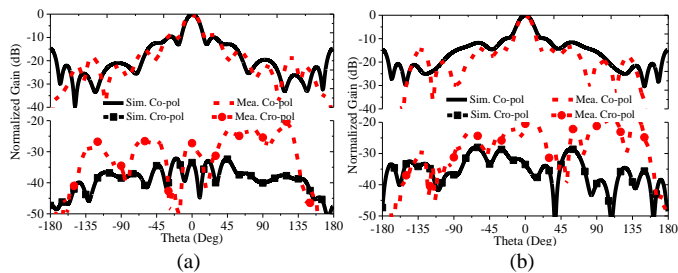

Fig. 19. Measured and simulated normalized radiation patterns of the proposed shared-aperture antenna at 10 GHz. (a). E-plane with Port 3 excited. (b). H-plane with Port 3 excited.
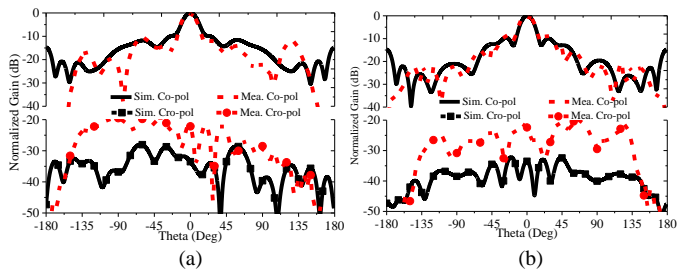

Fig. 20. Measured and simulated normalized radiation patterns of the proposed shared-aperture antenna at 10 GHz. (a). E-plane with Port 4 excited. (b). H-plane with Port 4 excited.

A. S-Parameters.

The S-parameters of the proposed shared-aperture antenna are measured with Keysight N5227A Power Network Analyzer (PNA). Firstly, the S-parameters of the proposed shared-aperture antenna in the low-frequency band is measured and shown in Fig. 18 (a), where the simulated results are also plotted for comparison. As seen in Fig. 18 (a), the measured and simulated results agree with each other well except for a small frequency shifting (around 50 MHz). The measured results show a -10-dB bandwidth of from 9.75 to 10.2 GHz with an absolute bandwidth of 450 MHz, the isolations between the two ports are better than 30 dB within the entire bandwidth.

The S-parameters of the proposed shared-aperture antenna in the high-frequency band are also measured. As seen in Fig. 18 (b), the measured results agree very well with the simulated ones, revealing a -10 dB bandwidth from 26.7 to 29.4 GHz with an absolute bandwidth of 2.7 GHz, and isolations between the two ports better than15 dB.

B. Realized gain and radiation patterns

According to the measured reflection coefficients, the radiation patterns and realized gains are all measured in an anechoic chamber. A dual-polarized horn antenna is used as a probe to measure the radiation patterns and realized gains of the proposed shared-aperture antenna. Besides, it should be mentioned that when one port is excited to measure the radiation patterns, the remaining ports in the low- and high-frequency bands are terminated with matching loads and the feeding cables for the high-frequecny band are also kept since the four ports of the shared-aperture antenna may be excited simultaneously in practical applications.

The normalized radiation patterns of the proposed shared-aperture antenna are evaluated at 10 GHz. Port 3 and Port 4 (see Fig. 17) are measured and shown in Fig. 19 and Fig. 20, respectively. The normalized co-polarizations of E- and H-plane are consistent between the simulated and measured results. The measured sidelobes are all better than -10 dB in both E- and H-plane. The measured normalized cross-polarizations in E- and H-plane are below -20 dB.

The normalized radiation patterns of the proposed shared-aperture antenna at 28 GHz are then measured. In order to minimize the blockage effects of the cables on the radiation patterns of the proposed shared-aperture antenna at 28 GHz, we fix the cables in the +/- 45 deg planes of the shared aperture to alleviate their effects on radiation patterns in E- and H-plane as much as possible. Fig. 21 and Fig. 22 show the measured normalized radiation patterns of Port 1 and Port 2, respectively. The simulated results are also plotted for comparison. It is observed that the co-polarizations of E- and H-plane between simulated and measured results are consistent with each other. Particularly, the measured main beam and the first radiation null are almost identical to the simulated counterparts. The measured sidelobes are all better than -18 dB in E- and H-plane. The measured normalized cross- polarizations of in E- and H-plane are all below -30 dB at 28 GHz.
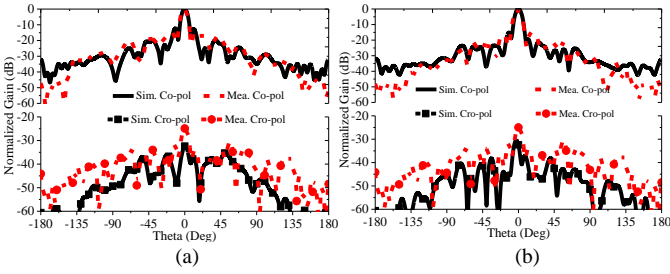
Fig. 21. Measured and simulated normalized radiation patterns of the proposed shared-aperture antenna at 28 GHz. (a). E-plane with Port 1 excited. (b). H-plane with Port 1 excited.
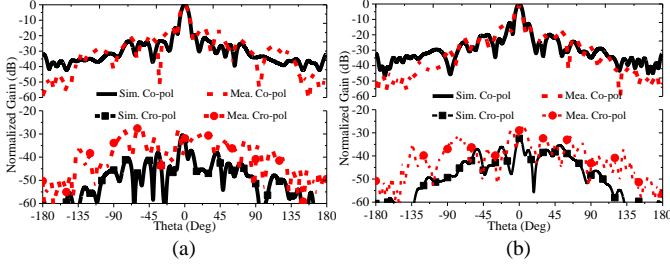

Fig. 22. Measured and simulated normalized radiation patterns of the proposed shared-aperture antenna at 28 GHz. (a). E-plane with Port 2 excited. (b). H-plane with Port 2 excited.

The realized gains of the proposed shared-aperture antenna in the low- and high-frequency band are also measured in the two orthogonal polarizations. It is found that the measured realized gains are highly consistent in the two polarizations both in low- and high-frequency band. Fig. 23 shows the measured realized gains over the frequencies from 8 to 12 GHz and 26 to 29 GHz in the polarization that Port 1 and Port 3 operate for brevity. The corresponding simulated results are presented for comparison. As seen in Fig. 23, the measured realized gains are 13.8 dBi at 10 GHz and 23.6 dBi at 28 GHz.
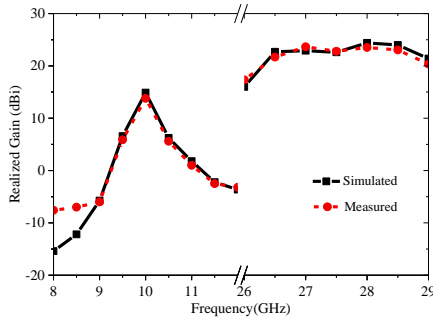

Fig. 23. Measured and simulated realized gains of the proposed shared-aperture antenna in the polarization that Port 1 and Port 3 operate.

Tab. Ⅲ Performance comparison of the proposed shared-aperture antenna with state-of-the-art and similar works

Ref	[1]	[2]	[5]	[6]	[11]	Proposed
f (GHz)	3.6; 25.8	3.6; 28	3.5; 60	5.3; 9.6	10.2; 22.0	10.0; 28.0
Gain (dBi)	10.88; 22.4	10.0; 14.0	7.3; 24	16.0; 20.0	26.2; 29.7	13.8; 23.6
*3dB	27%;	23.4%	5.7%;	4.7%;	16%;	6.0%;
bandwidth	5.8%	9.76%	3.3%	6.25%	9.1%	10.7%
#Pol	Single	Single	Single	Dual	Single	Dual
Size (mm * mm * mm)	90 * 90 * 6.9	92 * 92 * 7.34	80 * 86 * 2.6	140 * 140 * 31	300 * 300 * 245	85 * 85 * 17
Aperture Reuse Efficiency	–	0.425	0.77	–	1.00	1.00
Feeding Network	Yes	Yes	Yes	Yes	No	No
Type	§MS; Slot	Slot; FP	Patch; Slot Array	FP; FP	Reflect arrays	FP; Folded TA antenna

*: 3dB gain drop bandwidth; #: Polarization; §: metasurface antenna; -: the shared-aperture antenna radiates through the different physical apertures in two different bands.

Tab. Ⅲ compares the proposed shared-aperture antenna with other state-of-the-art and similar works on some figure of merits. It is observed that the proposed shared-aperture antenna is highlighted by its easy realizations of dual-polarization and high gain compared to references [1], [2], [5], [6] in which big footprint and complicated feeding networks are essential for dual-polarization and high gain implementations. In contrast, the proposed shared-aperture antenna does not need any feeding networks to achieve high gain and dual-polarization. The bandwidth of the proposed shared-aperture antenna in X-band is 6.0 %, which is mainly restricted by the inherently narrowband characteristics of a FP antenna that is typically characterized as a kind of resonant-based antenna. The similarly narrow bandwidths are also obtained in [2], [6], where FP antennas are adopted. It should be emphasized here that both of the feeding sources of the proposed shared-aperture antenna in X- and Ka-band radiate into free space through the physically same aperture like a dual-band reflectarray antenna reported in [11], resulting in a perfect aperture reuse efficiency. However, the dual-band reflectarray antenna in [11] suffers from the bulky volume (high profile) and high dependence of the two bands.

VI. CONCLUSIONS

A dual-polarized and high-gain X/Ka-band shared-aperture antenna with a perfect aperture reuse efficiency is proposed in this paper. It is the first attempt to combine a Fabry-Perot and a folded transmitarray antenna operating in X- and Ka-band, respectively, to form a shared-aperture antenna. To implement the required shared aperture, a four-layered double-ring-based unit cell is configured and analyzed, where it is found that frequency responses of the unit cell in the low- and high-frequency band are highly independent. Two dual-polarized patch antennas operating in X- and Ka-band are introduced to make the proposed shared-aperture antenna work in a dual-polarized manner. Since both of the two antennas radiate into free space through the same physical aperture, the aperture reuse efficiency of the proposed shared-aperture antenna is 100 %. The measured results are highly consistent with the simulated results, verifying the effectiveness of the proposed shared-aperture antenna.

REFERENCES

[1] T. Li, and Z. N. Chen, "Metasurface-based shared-aperture 5G S-/K-Band antenna using characteristic mode analysis," *IEEE Trans. Antennas and Propag.*, vol. 66, no. 12, pp. 6742-6750, Dec 2018.

[2] T. Li, and Z. N. Chen, "Shared-aperture dual-band antenna for 5G applications," *IEEE Trans. Antennas and Propag.*, vol. 68, no. 2, pp. 1128-67501133, Feb 2020.

[3] Y. Chen, and R. Vaughan, "Dual-polarized L-band and single-polarized X-band shared-aperture SAR array," *IEEE Trans. Antennas and Propag.*, vol. 66, no. 7, pp. 3391-3400, July 2018.

[4] T. Li, H. Meng, and W. Dou, "Design and implementation of dual-frequency dual-polarization slotted waveguide antenna array for Ka-band application," *IEEE Aantennas Wireless Propag. Lett.*, vol. 13, pp. 1317-1320, 2014.

[5] J. Zhang, Y. Cheng, Y. Ding, and C. Bai, "A dual-band shared-aperture antenna with large frequency ratio, high aperture reuse efficiency, and high channel isolation," *IEEE Trans. Antennas and Propag.*, vol. 67, no. 2, pp. 853-860, Feb 2019.

[6] F. Qin, S. Gao, Q. Luo, C. Mao, C. Gu, G. Wei, J. Xu, J. Li, C. Wu, K. Zheng, and S. Zheng, "A simple low-cost shared-aperture dual-band dual-polarized high-gain antenna for synthetic aperture radars," *IEEE Trans. Antennas and Propag.*, vol. 64, no. 7, pp. 2914-2922, July 2016.

[7] D. Pozar, and S. Targonski, "A shared-aperture dual-band dual-polarized microstrip array," *IEEE Trans. Antennas and Propag.*, vol. 49, no. 2, pp. 150-157, Feb 2001.

[8] L. Kong, and X. Xu, "A compact dual-band dual-polarized microstrip antenna array for MIMO-SAR applications," *IEEE Trans. Antennas and Propag.*, vol. 66, no. 5, pp. 2374-2381, May 2018.

[9] C. Mao, S. Gao, Q. Luo, T. Rommel, and Q. Chu, "Low-cost X/Ku/Ka-band dual-polarized array with shared aperture," *IEEE Trans. Antennas and Propag.*, vol. 65, no. 7, pp. 3520-3527, July 2017.

[10] J. Zhang, W. Wu, and D. Fang, "Dual-band and dual-circularly polarized shared-aperture array antennas with single-layer substrate," *IEEE Trans. Antennas and Propag.*, vol. 64, no. 1, pp. 109-116, Jan 2016.

[11] R. S. Malfaiani, and Z. Atlasbaf, "Design and implementation of a dual-band single layer reflectarray in X and Ka bands," *IEEE Trans. Antennas and Propag.*, vol. 62, no. 8, pp. 4425-4431, Aug 2014.

[12] Y. Chen, J. Zhao, and S. Yang, "A novel stacked antenna configuration and its applications in dual-band shared-aperture base station antenna array design," *IEEE Trans. Antennas and Propag.*, *IEEE Trans. Antennas and Propag.*, vol. 67, no. 12, pp. 7234-7241, Feb 2019.

[13] K. Naishadham, R. Li, L. Yang, T. Wu, W. Hunsicker, and M. Tentzeris, "A shared-aperture dual-band planar array with self-similar printed folded dipoles," *IEEE Trans. Antennas and Propag.*, vol. 61, no. 2, pp. 606-613, Feb 2013.

[14] A. Abdelrahman, A. Elsherbeni, and F. Yang, "Transmission phase limit of multilayer frequency selective surfaces for transmitarray designs," *IEEE Trans. Antennas Propag.*, vol. 62, no.2, pp. 690-697, Feb 2014.

[15] D. M. Pozar, "*Microwave Engineering*," 3rd, John Wwiley & Sons, Inc., New York, 2005.

[16] P. Mei, S. Zhang, X. Lin, and G. F. Pedersen, "Design of an absorptive Fabry-Perot polarizer and Its application on antenna," *IEEE Aantennas Wireless Propag. Lett.*, vol. 18, no.7, pp. 1352-1356, July 2019.

[17] N. Nguyen-Trong, H. Tran, T. Nguyen, and A. Abbosh, "Wideband Fabry-Perot antennas employing multilayer of closely spaced thin dielectric slabs," *IEEE Aantennas Wireless Propag. Lett.*, vol. 17, no.7, pp. 1354-1358, July 2018.

[18] N. Guerin, S. Enoch, G. Tayeb, P. Sabouroux, P. Vincent, and H. Legay, "A metallic Fabry-Perot directive antenna," *IEEE Trans. Antennas Propag.*, vol. 54, no. 1, pp. 220-224, Jan. 2006.

[19] J. S. Colburn, Y. R. Samii, "Patch antennas on externally perforated high dielectric constant substrates," *IEEE Trans. Antennas Propag.*, vol. 47, no. 12, pp. 1785-1794, Dec. 1999.

[20] J. Huang, "The finite ground plane effect on the microstrip antenna radiation patterns," *IEEE Trans. Antennas Propag.*, vol. AP-31, pp. 649-653, July. 1983.

[21] G. V. Trentini, "Partially reflecting sheet arrays," *IRE Trans. Antennas Propag.*, vol. AP-4, no. 4, pp. 666-671, Oct. 1956.

[22] https://fractory.com/cnc-milling/